

Lawrence Berkeley National Laboratory

LBL Publications

Title

Periodic Trends in Actinyl Thio-Crown Ether Complexes

Permalink

<https://escholarship.org/uc/item/1611z8r0>

Journal

Inorganic Chemistry, 57(5)

ISSN

0020-1669

Authors

Hu, Shu-Xian

Liu, Jing-Jing

Gibson, John K

et al.

Publication Date

2018-03-05

DOI

10.1021/acs.inorgchem.7b03277

Copyright Information

This work is made available under the terms of a Creative Commons Attribution-NonCommercial-NoDerivatives License, available at

<https://creativecommons.org/licenses/by-nc-nd/4.0/>

Peer reviewed

Periodic Trends in Actinyl Thio-crown Complexes

Shu-Xian Hu,¹ Jing-Jing Liu,² John K. Gibson,^{3*} and Jun Li^{2*}

¹ Beijing Computational Science Research Center, Beijing 100193, China.

² Department of Chemistry and Key Laboratory of Organic Optoelectronics & Molecular Engineering of Ministry of Education, Tsinghua University, Beijing 100084, China.

³ Chemical Sciences Division, Lawrence Berkeley National Laboratory, Berkeley, California 94720, United States.

*Corresponding authors. E-mail: jkgibson@lbl.gov (Gibson); junli@tsinghua.edu.cn (Li).

Abstract. Actinyl(VI) (An = U, Np, Pu, Am and Cm) complexes of thio-crown (TC) ethers have been characterized using density functional theory. On the basis of the calculations, the “double-decker” sandwich structure of $\text{AnO}_2(12\text{TC4})_2^{2+}$ and “side-on” structure $\text{AnO}_2(12\text{TC4})^{2+}$ are replaced by “standing” inclusion structures for $\text{AnO}_2(15\text{TC5})^{2+}$ and $\text{AnO}_2(18\text{TC6})^{2+}$. The actinyl monocyclic ether complexes are found to exhibit conventional conformations, with typical An–O_{actinyl} and An–S_{ligand} distances and angles. Bonding analysis by Weinhold’s natural population analysis (NPA), natural localized molecular orbital (NLMO) and electronic decomposed analysis (EDA), shows that a typical ionic An–S_{ligand} bond with the extent of covalent interaction between the An and S atoms due to the extent of radial distribution of the S-3p atomic orbitals. As soft S-donor ligands, TC ethers may be candidate ligands for actinide recognition and extraction.

Introduction

Actinide complexes are of both fundamental and practical interest, owing to their prevalence in the nuclear energy industry, which is an important source of electricity.[1-3] Therefore, issues related to nuclear fuel reprocessing and waste storage have to be addressed. Nuclear waste typically contains both actinides (mostly U, Np, Pu, Am, Cm) and their fission products (including lanthanides, Cs, Tc) in an aqueous environment.[4] The treatment of nuclear waste, involving either separation of the actinides as useful commodities or their immobilization for long-term storage, is dominated by interactions with water.[5-8]

In aqueous solutions, uranium complexes exist mostly in the form of $\text{U}^{\text{VI}}\text{O}_2^{2+}$, whereas $\text{Np}^{\text{VI}}\text{O}_2^{2+}$ and $\text{Pu}^{\text{VI}}\text{O}_2^{2+}$ are substantially less stable, and AmO_2^{2+} is metastable.[9-13] Published structural data

reveal a smooth actinide contraction of actinyl bond lengths from $R(\text{U}-\text{O}) = 180 \text{ pm}$ to $R(\text{Am}-\text{O}) = 175 \text{ pm}$. [14-17] The existence of CmO_2^{2+} in solution has not yet been reliably demonstrated and this species is considered unimportant in curium chemistry. [18, 19] The actinyl moiety is remarkable due to the fact that it is, in contrast to similar d-element compounds, linear and has very short metal-oxygen bond lengths, suggesting strong multiple bond character. Actinyl complexes normally coordinate 4-6 monodentate ligands in their equatorial plane. [20-24] The f-elements, in contrast to many d-block transition metals, are in general hard acids and therefore have a strong affinity for hard O- and F-donor ligands. The choice of donor atoms has been a hot topic in the rational design of actinide separation or sequestering ligands. [25-27] It is well-known that actinides form somewhat more covalent bonds than lanthanides and therefore have slightly better affinities for soft bases such as S-donor ligands. [28] This could potentially be exploited in the separation of actinide from lanthanide cations. [29-31] One of the methods proposed for nuclear waste treatment involves the coordination of actinide ions by polydentate macrocyclic ligands, thus exploiting the chelate effect. [32, 33] Moreover, macrocyclic ligands could potentially be tuned to provide the best fit for specific cations and oxidation states by varying the size of the ligand's inner cavity. [34] There are many types of macrocyclic ligands known to date with much attention having focused on N-donor ligands. Another important family of macrocyclic ligands are crown ethers and thio-crown ethers, the capacity of which to form stable complexes with transition metals is well-known. [35, 36] Recently, several studies of crown ethers, both experimental and theoretical, have reported on the structural characterization, [37] the equatorial bonding properties of the actinyl cations, and bonding trends across the actinyl series. [6, 38] However, in-cavity complexes and the corresponding bonding features between thio-crown ethers and f-elements are essentially unexplored.

Theoretical studies on the factors determining the stability and bonding interactions between actinyls and thio-crown ethers could help in the development of new, more efficient separations processes, and could elucidate the failure to prepare Cm^{VI} and other late actinyl analogues. In this study, a series of $\text{AnO}_2(\text{L})_2^{2+}$ complexes ($\text{An} = \text{U}$ through Cm ; $\text{L} =$ tetrathio-12-crown-4 (12TC4), pentathio-15-crown-5 (15TC5) and hexathio-18-crown-6 (18TC6) have been systematically explored using density functional theory (DFT). The structural parameters and their dependence on solvent interactions have been examined. The orbital interactions and between actinyls and the coordinating ligands, and the bonding trends across the serial from $\text{An} = \text{U}$ to Cm , have been elucidated using

various bonding analysis approaches.

2. METHODOLOGY

Calculations of the $\text{AnO}_2(\text{L})_n^{2+}$ ($\text{An} = \text{U}, \text{Np}, \text{Pu}, \text{Am}$ and Cm ; $n = 1, 2$; $\text{L} = 12\text{TC}4, 15\text{TC}5$ and $18\text{TC}6$ complexes, their decomposed products, and the various ligands were carried out using spin-unrestricted Kohn–Sham DFT. The scalar relativistic DFT calculations were performed with the Gaussian 09[39] and ADF software[40, 41] for the geometry optimizations and vibrational frequency analyses. The geometry optimizations, Mulliken population analysis[42] and the binding energy analysis were initially carried out using the local density approximation (LDA)[43] and generalized gradient approach with PBE exchange-correlation functional[44] as implemented in ADF 2016.106. The scalar zeroth-order regular approximation (ZORA)[45, 46] was used in conjunction with Slater type orbitals (STOs)[47] of the quality of triple-zeta plus polarization functions (TZP), and double- ζ plus polarization functions (DZP) were used for the valence electrons of the actinyls and crown ethers, respectively. The frozen core approximation was applied to the $[1s^2-5d^{10}]$ cores of U, Np, Pu, Am and Cm, the $[1s^2]$ cores of C and O, and the $[2p^6]$ cores of S, with the rest of the electrons explicitly treated variationally. The geometry optimizations were performed without symmetry restrictions and were followed by vibrational frequency analysis to determine the local minima or saddle point natures of the optimized structures. The conductor-like screening solvation model (COSMO)[48] was employed to consider the effects of water on the electronic and geometric structures of the complexes. The following atomic COSMO-default radii from the ADF code were used: Pu 210.0 pm, Am 210.0 pm, C 170.0 pm, S 179.2 pm, O 151.7 pm, and H 135.0 pm.[49] The reported reaction energies were obtained by combining the electronic energies with the zero-point vibrational energy corrections. The energy decomposition analyses (EDA)[50, 51] and combined extended transition state (ETS)[52] with the natural orbitals for chemical valence (NOCV) theory was carried out.[50, 53, 54] Bond order analyses was performed based on the Mayer method (BO_{Mayer})[55], and Nalewajski-Mrozek method (BO_{NM})[53, 54, 56, 57]. The electron localization functions (ELF)[58] were calculated to investigate the features of the weak dative bonding.

In further geometry optimizations using Gaussian code, we used the scalar relativistic Stuttgart energy-consistent relativistic 32-valence-electron pseudopotential and associated ECP60MWB_SEG valence basis set[59-61] for the actinide atoms. The Dunning's correlation consistent basis set with

polarized triple-zeta (cc-pVTZ)[62] were used for the oxygen, carbon and hydrogen atoms. The B3LYP hybrid density functional[63, 64] was used in these calculations. The combination of these pseudopotential and basis sets with this functional (labeled as B3LYP/ECP60MWB_SEG/cc-pVTZ level) has been shown to give accurate predictions of the properties and reaction energies of actinide complexes. The Weinhold's natural bond orbitals (NBO)[65] and natural localized molecular orbital (NLMO)[66] analyses were performed at the B3LYP/6-31G* level[67] on optimized geometries from B3LYP calculations by using the NBO 5.0 program.[68]

3. RESULTS AND DISCUSSION

3.1. Structures and Stability of the $\text{AnO}_2(12\text{TC4})_2^{2+}$ and $\text{AnO}_2(12\text{TC4})_2^{2+}$.

The theoretically optimized stable structures of the $\text{AnO}_2(12\text{TC4})_2^{2+}$ ($\text{An} = \text{U}, \text{Np}, \text{Pu}, \text{Am}, \text{Cm}$) complexes are shown in Figure 1 (the $\text{AnO}_2(12\text{TC4})_2^{2+}$ structures are in SI Figure S1); the structures of the complexes for all five An are similar. The actinide metal center prefers coordination by the four S atoms in a “double decker” structure rather than in-cavity “standing” structures as identified below for other complexes. As apparent in Figures 1 and S1, the actinyl resides above the 12TC4 ligand in $\text{AnO}_2(12\text{TC4})_2^{2+}$ and lies between two ligands in $\text{AnO}_2(12\text{TC4})_2^{2+}$. These types of structures are usually rationalized as misfit of actinyl cation with the inner cavity of a crown ether ligand that is too small to accommodate the actinyl or other cation. In the “double decker” structure of $\text{AnO}_2(12\text{TC4})_2^{2+}$ (Table 2), the actinyl is coordinated by four crown ether S atoms (D_2 symmetry) from two 12TC4 (two S atoms of each ether) with An–S bond distances around 3.0 Å, which suggests weak bonding interactions. All the An-S bond lengths in the complexes are beyond the range of M–S covalent single-bond lengths estimated by the sum of the self-consistent covalent radii derived by Pyykkö,[69] indicating predominantly dative bonding. The calculated An–O distances decrease from uranium, where the U–O bond lengths are 1.796 Å, to plutonium, where the Pu–O bond lengths are 1.777 Å, and then increase to curium, where the Cm–O bond lengths are 1.812 Å. This plutonium turn coincides with results from our previous work.[6, 22] The change in O-An-O bond angle from highly bent for U to linear for Am and Cm is due to gradually weaker bonding to S atoms in 12TC4, as indicated by increasing An-S bond distance and decreasing static interaction between actinyl and thio-crown ether from U to Cm.

In contrast to the “double decker” structures of the $\text{An}^{\text{VI}}\text{O}_2(12\text{TC4})_2^{2+}$ complexes, in the

“side-on” structure of $\text{UO}_2(12\text{TC4})_2^{2+}$, the uranyl is coordinated to four S atoms (C_2 symmetry) with U–S bond lengths of 2.931 Å and 3.069 Å (Table 2). Notably, the An coordination number decrease from four in $\text{UO}_2(12\text{TC4})_2^{2+}$ to two in $\text{CmO}_2(12\text{TC4})_2^{2+}$ with average An–S distances increasing from 3.000 Å to 3.377 Å, likely due to decreasing charge and that the contracted 5f/6d orbitals leads to weaker bonding from U to Cm. The calculated An–O distances decrease from uranium, where the U–O bond lengths are around 1.796 Å, to americium, where the Am–O bond lengths are around 1.766 Å, as expected based on the decrease in atomic radii across the series. The distance increases for curium to Cm–O bond lengths around 1.794 Å, as expected due to the decrease of ionic and covalent bonding. A substantial energy of around 60 kcal/mol (Table 1) is released upon binding of $\text{An}^{\text{VI}}\text{O}_2(12\text{TC4})_2^{2+}$ to another 12TC4 ether to form $\text{An}^{\text{VI}}\text{O}_2(12\text{TC4})_2^{2+}$. The initial $\text{An}^{\text{VI}}\text{O}_2(12\text{TC4})_2^{2+}$ complex can be considered as an intermediate along the reaction path of $\text{An}^{\text{VI}}\text{O}_2^{2+} + 2(12\text{TC4}) \rightarrow \text{An}^{\text{VI}}\text{O}_2(12\text{TC4})_2^{2+}$; the electronic structure and bonding feature discussions for $\text{An}^{\text{VI}}\text{O}_2(12\text{TC4})_2^{2+}$ are not presented in the main text but can be found in supporting information.

Because these f-element complexes are predominantly ionic, and nuclear fuel reprocessing is usually involve aqueous solutions, polarized solvation effects of water by using the COSMO model have been considered on the geometrical structure of the $\text{AnO}_2(12\text{TC4})_2^{2+}$ (An = U, Np, Pu, Am and Cm) complexes. Since solvation minimally affects the coordination and gives essentially the same structure trends, the following computational decomposition of the bonding was performed in the gas phase. In addition to ionic interactions between ligands and the actinyl (VI) cations, some insights are presented for charge transfer and polarization effects.

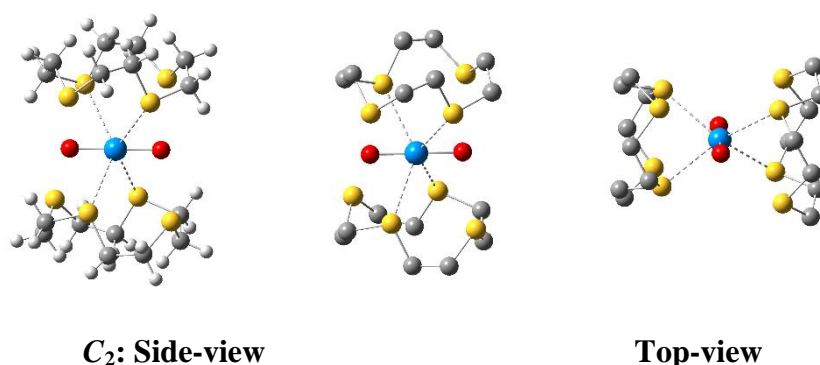


Figure 1. Optimized geometry of $\text{AnO}_2^{2+}(12\text{TC4})_2$ by using PBE/TZP/DZP.

Table 1. Relative energy (ΔE , kcal/mol) of side-on and standing isomers, and binding energy (presented as the negative of the bond dissociation energy, -BDE) for the formation of $\text{AnO}_2^{2+}(\text{12TC4})$ and $\text{AnO}_2^{2+}(\text{12TC4})_2$ from isolated AnO_2^{2+} and 12TC4 fragments at PBE/TZP/DZP level.

	$\text{AnO}_2^{2+}(\text{12TC4})$						$\text{AnO}_2^{2+}(\text{12TC4})_2$					
	side-on		standing		side-on		double-decker		standing		double-decker	
	ΔE		ΔE		-BDE		ΔE		ΔE		-BDE	
An	SR	SO	SR	SO	SR	SO	SR	SO	SR	SO	SR	SO
U	0.00	0.00	17.30	27.37	-198.69	-200.67	0.00	0.00	31.30	34.10	-269.97	-272.05
Np	0.00	0.00	18.37	34.10	-198.59	-198.48	0.00	0.00	34.72	27.50	-267.42	-267.73
Pu	0.00	0.00	21.20	27.50	-195.15	-193.49	0.00	0.00	30.86	29.26	-263.94	-262.71
Am	0.00	0.00	10.61	29.26	-193.76	-192.02	0.00	0.00	28.87	31.01	-266.10	-264.61
Cm	0.00	0.00	7.22	31.01	-182.29	-187.9	0.00	0.00	29.01	27.37	-255.98	-260.00

* $\Delta E = E[\text{side-on}] - E[\text{standing}]$ for $\text{AnO}_2(\text{12TC4})^{2+}$ and $\Delta E = E[\text{double-decker}] - E[\text{standing}]$ for $\text{AnO}_2(\text{12TC4})_2^{2+}$; $\text{BDE} = E[\text{AnO}_2(\text{12TC4})^{2+}] - E[\text{AnO}_2^{2+}] - E[\text{12TC4}]$.

Table 2. Selected average bond length (\AA) and $\text{O}\equiv\text{An}\equiv\text{O}$ bond angle ($^\circ$) of the ground state D_2 $\text{AnO}_2^{2+}(\text{12TC4})_2$ in vacuum and in water considered by COSMO solvation model (in parentheses) at PBE/TZP/DZP level.

An	Spin State	Point group	Elec. Conf.	Bond length		Bond angle
				$\text{An}\equiv\text{O}$	4^*An-S	$\text{O}\equiv\text{An}\equiv\text{O}$
U	1	C_2	f^0	1.796 (1.799)	3.075 (3.067)	144.0 (147.8)
Np	2	C_2	f_ϕ^1	1.793 (1.795)	3.024 (2.993)	151.6 (150.3)
Pu	3	C_2	$f_\phi^1 f_\delta^1$	1.777 (1.779)	3.002 (2.991)	163.1 (161.6)
Am	4	C_2	$f_\phi^1 f_\delta^2$	1.780 (1.777)	2.989 (2.958)	180.0 (179.0)
Cm	5	C_2	$f_\phi^2 f_\delta^2$	1.812 (1.806)	3.022 (3.004)	180.0 (179.7)

* An-S bond distances larger than 3.7 \AA are not listed.

3.2. Structures and Stability of the $\text{AnO}_2(\text{15TC5})^{2+}$ and $\text{AnO}_2(\text{15TC5})_2^{2+}$.

The geometrical optimization for the $\text{An}^{\text{VI}}\text{O}_2(\text{15TC5})^{2+}$ and $\text{An}^{\text{VI}}\text{O}_2(\text{15TC5})_2^{2+}$ ($\text{An} = \text{U}, \text{Np}, \text{Pu}, \text{Am}$ and Cm) complexes have been explored. The $\text{An}^{\text{VI}}\text{O}_2(\text{15TC5})_2^{2+}$ are unstable with a large imaginary frequency, leading to the formation of the $\text{An}^{\text{VI}}\text{O}_2(\text{15TC5})^{2+}$ shown in Figure 2. $\text{An}^{\text{VI}}\text{O}_2^{2+}$

prefers coordination by one rather than two 15TC5; this is considered as due to a weak bonding interaction of metal and sulfur atoms and large steric repulsion between two 15TC5 ligands. In contrast to the “side-on” structure of $\text{AnO}_2(12\text{TC4})_2^{2+}$ or “double-decker” structure of $\text{AnO}_2(12\text{TC4})_2^{2+}$, the ground state structures of the $\text{AnO}_2(15\text{TC5})_2^{2+}$ is a “standing” structure, in which the actinyl coordinates to all five S atoms with the average An–S distance decreasing from 2.931 Å in An = U to 2.902 Å in An = Cm (Table 3). This variation is attributed to the relativistic contraction of the An ionic radius. As was found for our previously studied oxo-crown complex, $\text{An}^{\text{VI}}\text{O}_2(15\text{C5})_2^{2+}$ (An = U, Np, Pu, Am and Cm), the AnO_2^{2+} is similarly trapped in the center of 15TC5 with a longer An–S distance than the range of the An–S covalent single-bond lengths estimated by the sum of the self-consistent covalent radii derived by Pyykkö[69]. The calculated An–O_{y1} distances in $\text{AnO}_2(15\text{TC5})_2^{2+}$ decrease from uranium (average U–O distance ≈ 1.789 Å), to americium, whereas the average An–O bond length is around 1.765 Å, and then increase up to curium, whereas the average An–O bond lengths are around 1.775 Å, as the results of balance between the contraction in atomic radii and bonding feature. Consistent with that of $\text{AnO}_2(12\text{TC4})_2^{2+}$, the well-known change from d-type dominance in charge of An=O bonding and then to f-type behavior is labeled as the americium turn, a phenomenon that is caused by f-orbital energy-decrease and f-orbital localization with increase of both nuclear charge and oxidation state, and a non-linear variation of effective f-electron population across the actinide series.[70]

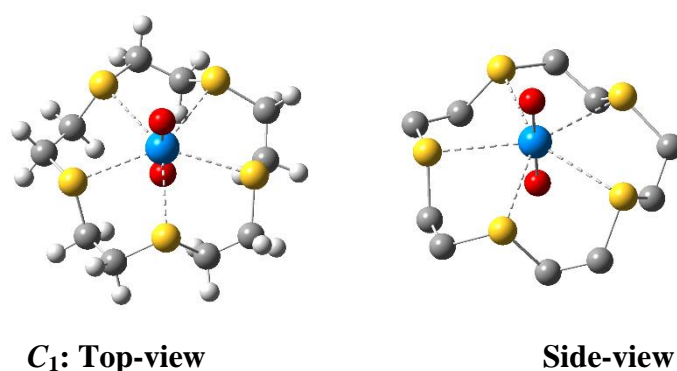


Figure 2. Optimized geometry of $\text{AnO}_2^{2+}(15\text{TC5})_2$ by using PBE/TZP/DZP.

Table 3. Selected average bond length (Å), $\text{O}\equiv\text{An}\equiv\text{O}$ bond angle ($^\circ$) and calculated vibrational

frequencies (cm^{-1}) and intensities (in parentheses, km/mol) of the ground state *Standing* $\text{AnO}_2^{2+}(15\text{TC5})$ in vacuum and in water considered by COSMO solvation model (in parentheses) and binding energy (-BDE, kcal/mol) of $\text{AnO}_2^{2+} + 15\text{TC5} = \text{AnO}_2^{2+}(15\text{TC5})$ at PBE/TZP/DZP level.

An	Spin State	Point group	Bond length		Bond angle	-BDE		O≡An≡O Stretch	
			An≡O	An-S	O≡An≡O	SR	SO	Asym.	Sym.
U	1	C_1	1.778, 1.799 (1.786,1.792)	2.931 (2.931)	180.0 (180.0)	-245.0	-251.1	970(142)	858(4)
Np	2	C_1	1.762, 1.782 (1.771,1.776)	2.921 (2.921)	180.0 (179.9)	-240.6	-245.6	966(131)	847(3)
Pu	3	C_1	1.761, 1.774 (1.766,1.768)	2.915 (2.919)	180.0 (179.8)	-245.2	-249.0	957(124)	829(1)
Am	4	C_1	1.756, 1.774 (1.763,1.767)	2.906 (2.913)	180.0 (178.6)	-242.5	-245.7	936(101)	796(1)
Cm	5	C_1	1.770, 1.779 (1.772,1.775)	2.902 (2.904)	180.0 (180.0)	-231.8	-239.8	898(60)	749(1)

3.3. Structures and Stability of the $\text{AnO}_2(18\text{TC6})^{2+}$.

As for 15TC5, $\text{An}^{\text{VI}}\text{O}_2(18\text{TC6})_2^{2+}$ is unstable relative to decomposition to $\text{An}^{\text{VI}}\text{O}_2(18\text{TC6})^{2+}$ and 18TC6. The optimized structures of the $\text{An}^{\text{VI}}\text{O}_2(18\text{TC6})^{2+}$ ($\text{An} = \text{U}, \text{Np}, \text{Pu}, \text{Am}$ and Cm) complexes are similar and displayed in Figure 3. The An-S distances are longer than 3.0 Å (Table 4), indicating a weaker interaction between An and $\text{S}_{18\text{TC6}}$ than between An and $\text{S}_{12\text{C4}}$ or $\text{S}_{15\text{C5}}$, which is confirmed from average Mayer bond order value of 0.3, 0.4 and 0.5 for An-S_{18C6}, An-S_{15C5}, and An-S_{12C4}, respectively. The turning-point of An-O_{yl} bond lengths occurs at An = Am, in agreement with the above results in $\text{An}^{\text{VI}}\text{O}_2(12\text{C4})^{2+}$ and $\text{An}^{\text{VI}}\text{O}_2(15\text{TC5})^{2+}$, and shifted up from the turn at Pu in the oxygen-containing complexes, which is consistent with the appearance of the turn at AmO_2^{2+} in isolated actinyls (Table 5), indicating weak ligand field effect of sulfur on $\text{An}^{\text{VI}}\text{O}_2^{2+}$.

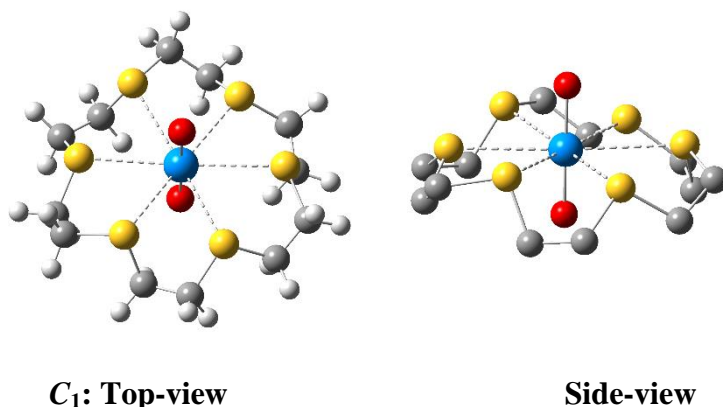


Figure 3. Optimized geometry of $\text{AnO}_2^{2+}(\text{18TC6})$ by using PBE/TZP/DZP.

Table 4. Selected average bond length (\AA) and $\text{O}\equiv\text{An}\equiv\text{O}$ bond angle ($^\circ$) and calculated vibrational frequencies (cm^{-1}) and intensities (in parentheses, km/mol) of the ground state *Standing* $\text{AnO}_2^{2+}(\text{18TC6})$ in vacuum and in water considered by COSMO solvation model (in parentheses) and binding energy (BDE, kcal/mol) of $\text{AnO}_2^{2+} + 18\text{TC6} = \text{AnO}_2^{2+}(\text{18TC6})$ at PBE/TZP/DZP level.

An	Spin State	Point group	Bond length		Bond angle	BDE		$\text{O}\equiv\text{An}\equiv\text{O}$ stretch	
			$\text{An}\equiv\text{O}$	An-S	$\text{O}\equiv\text{An}\equiv\text{O}$	SR	SO	sym.	asym.
U	1	C_1	1.781,1.798 (1.791,1.796)	3.090 (3.070)	180.0 (179.8)	-265.3	-271.6	861(2)	963(150)
Np	2	C_1	1.765,1.782 (1.774,1.780)	3.088 (3.070)	179.8 (179.6)	-260.8	-265.0	851(2)	962(139)
Pu	3	C_1	1.761,1.775 (1.766,1.772)	3.080 (3.069)	179.3 (179.7)	-262.4	-266.0	817(2)	952(118)
Am	4	C_1	1.760,1.775 (1.767,1.773)	3.098 (3.080)	179.8 (179.8)	-266.2	-267.2	794(2)	929(102)
Cm	5	C_1	1.778,1.798(1.788,1.797)	3.142 (3.131)	179.8 (179.9)	-243.9	-251.7	720(0)	872(73)

Table 5. An-O bond length (\AA) of isolated AnO_2^{2+} at different density functionals along with T2ZP basis set for all atoms.

	LDA	PBE	PBE0	HF	SO-CASPT2
U	1.700	1.716	1.686	1.654	1.710
Np	1.698	1.714	1.679	1.641	1.700
Pu	1.685	1.703	1.666	1.627	1.675
Am	1.675	1.695	1.652	1.649	1.679
Cm	1.687	1.712	1.674	1.989	1.674

The structural results indicate that the average metal–ligand distances increase in the order $An-S_{12C4} > An-S_{L2} < An-S_{L3}$. The fact that the $An-S_{L2}$ bond lengths are shorter than those of $An-S_{L3}$ is due to the smaller cavity radius of 15-thio-crown-5 ether. The shorter $An-S_{L2}$ bond length compared with $An-S_{L1}$ can be partially ascribed to their different coordination structures.

3.4. Electronic structure and bonding analyses of $AnO_2^{2+}(L)_n$.

Insights into the involvement of the 5f orbitals in bonding were obtained through electronic structure analyses of $AnO_2(15TC5)^{2+}$ at the B3LYP/TZ2P level. Selected molecular orbitals in the HOMO–LUMO region involving the 5f orbitals are depicted as the energy levels of 5f-, 6d- and 7s-based MOs of the actinides fragment together with the S-3p orbitals in Figure 4. The MOs from the S-3p are fully occupied, and the highest singly occupied α spin orbitals (SOMOs) are occupied in An. The An-6d and An-7s AOs slightly increase in energy through U to Cm, while the 5f orbitals significantly decrease in energy so they become nearly degenerate with the sulfur lone-pair orbitals. The An 5f orbitals are stabilized so much so that they eventually lie below the ligand orbitals beyond Am, which explains the difficulty for the formation of higher oxidation states for the later actinide elements. This general trend has been observed in a number of actinide complexes with different ligands, thus being a general feature of actinide chemistry. In contrast to the significant hybridization at $An = Am$ with oxygen ligand, An-5f and S-3p AOs mix strongly due to the higher energy level of S-3p AOs than that of O-2p.

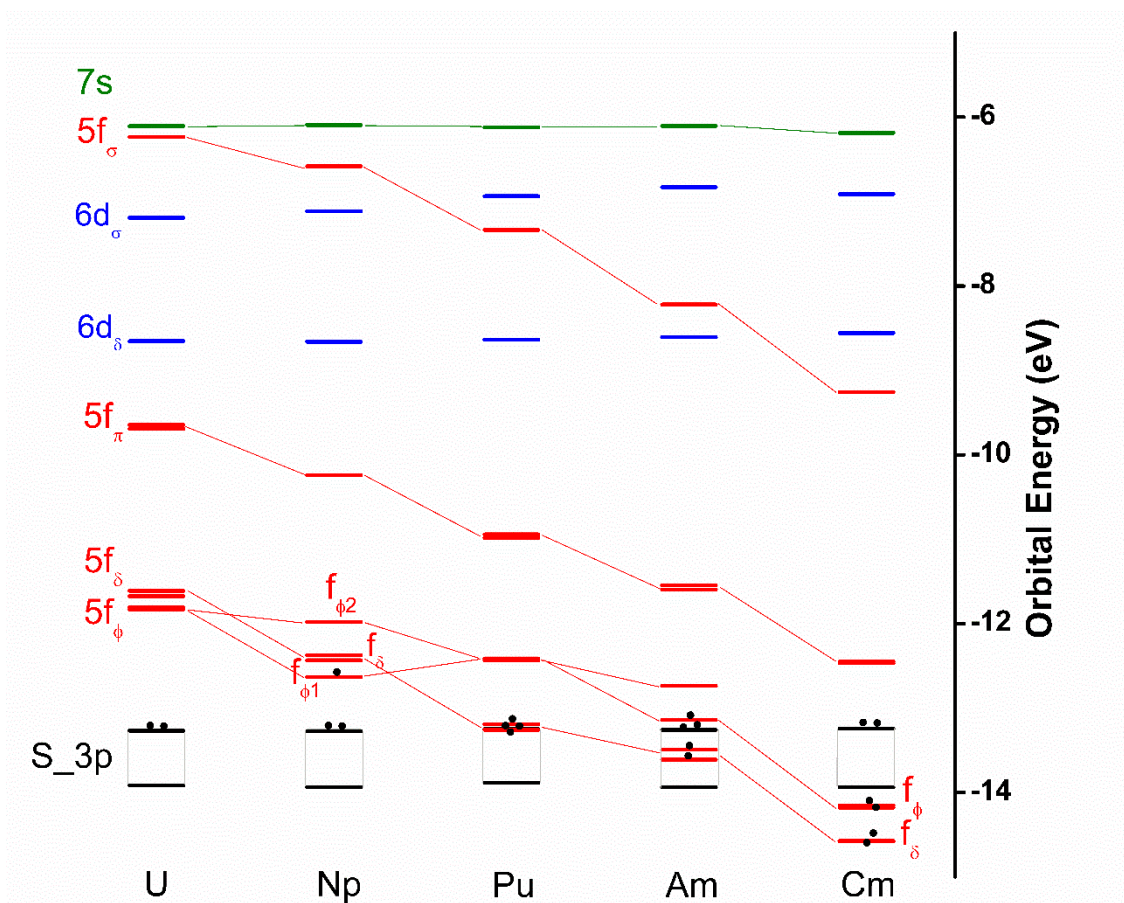


Figure 4. Scalar relativistic KS-PBE molecular orbital energy levels of free $\text{AnO}_2(15\text{TC5})^{2+}$ ions for $\text{An} = \text{U}, \text{Np}, \text{Pu}, \text{Am},$ and Cm .

The ETS-NOCV analysis (Table 6) was carried out in order to reveal the intrinsic bonding mechanism in terms of the major contributions to the orbital interactions. The degree of ionicity and covalency of the An-S_L bond in $\text{AnO}_2(\text{L})^{2+}$ ($\text{An} = \text{U}, \text{Np}, \text{Pu}, \text{Am}, \text{Cm}$) has been evaluated by a quantitative index. The trend of increasing covalent character through U to Cm in all the studied complexes can be understood in terms of energy degeneracy of S-3p and An-5f AOs, and the extend radial distribution of S-3p AOs that favor large orbital overlap, which contributes to a considerable energetic stabilization. In contrast to the covalency, the ionic character for these complexes has an opposite trend of decreasing from U to Cm. Thus, the chemical bonding of actinyl and thio-crown ether ligand features a turning-point at $\text{An} = \text{Am}$, as a result of balancing between the decreasing ionic dative bonding and the increasing covalent interaction. Irrespective of structure and actinide metal, the An 5f/6d orbitals are mainly localized on the metal site (see the plot of representative An-S_L bonding interaction from ETS-NOCV method in Figures 5, 6 and 7), respectively. There is quite few evident interaction of the An 5f orbitals with any coordinating sulfur atoms of the

thio-crown ether ligands. Additional electron localization function (ELF, Figures 8-10) analyses reveals that despite that these terminal An–S_L bonds are primarily centered on the An and S_L atoms the An–S_L dative bonds possess essentially ionic character in the bonding interactions.

Table 6. EDA and ETS-NOCV analysis of AnO₂(12TC4)₂²⁺, AnO₂(15TC5)²⁺ and AnO₂(18TC6)²⁺ (An = U, Np, Pu, Am and Cm) complexes at PBE/T2ZP level of theory.

	Pauli Repulsion	Electrostatic Interaction	Orbital Interactions	Bonding Energy	Covalency
AnO ₂ (12TC4) ₂ ²⁺					
U	182.28	-193.05	-242.25	-253.01	0.56
Np	165.90	-189.53	-260.42	-284.06	0.58
Pu	140.86	-176.58	-259.76	-295.49	0.60
Am	136.52	-172.34	-304.00	-339.84	0.64
Cm	141.08	-179.13	-317.42	-355.49	0.64
AnO ₂ (15TC5) ²⁺					
U	212.95	-210.78	-255.04	-252.86	0.55
Np	206.75	-208.82	-253.76	-255.83	0.55
Pu	199.39	-206.17	-281.63	-288.41	0.58
Am	193.78	-201.69	-304.13	-312.04	0.60
Cm	187.01	-201.84	-325.25	-340.08	0.62
AnO ₂ (18TC6) ²⁺					
U	133.88	-171.43	-243.42	-280.97	0.59
Np	127.39	-168.47	-270	-311.08	0.62
Pu	123.79	-166.93	-267.89	-311.04	0.62
Am	111.97	-161.07	-312.13	-361.24	0.66
Cm	111.73	-159.80	-307.42	-355.50	0.66

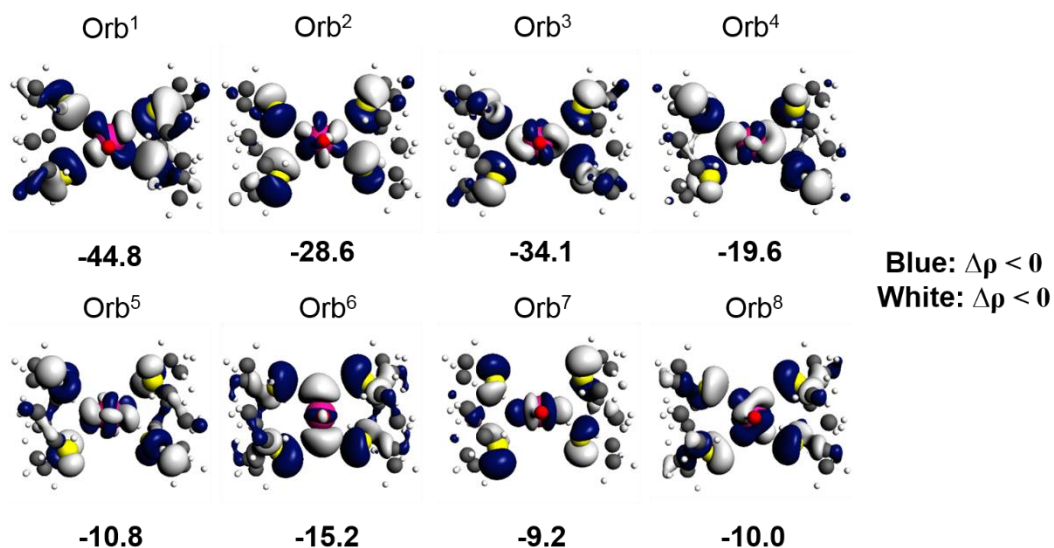


Figure 5. Plot of representative An-S_{L1} bonding interactions from ETS-NOCV method from an open-shell B3LYP calculation (energy unit: kcal/mol, isovalue=0.03).

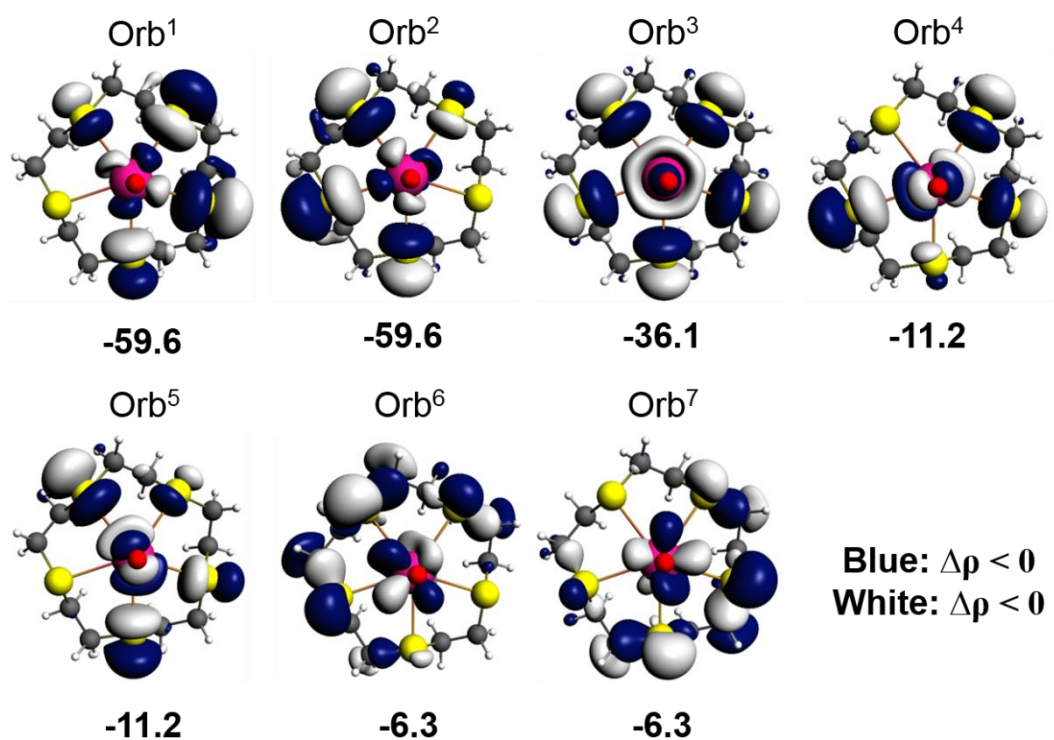


Figure 6. Plot of representative An-S_{L2} bonding interactions from ETS-NOCV method from an open-shell B3LYP calculation (energy unit: kcal/mol, isovalue=0.03).

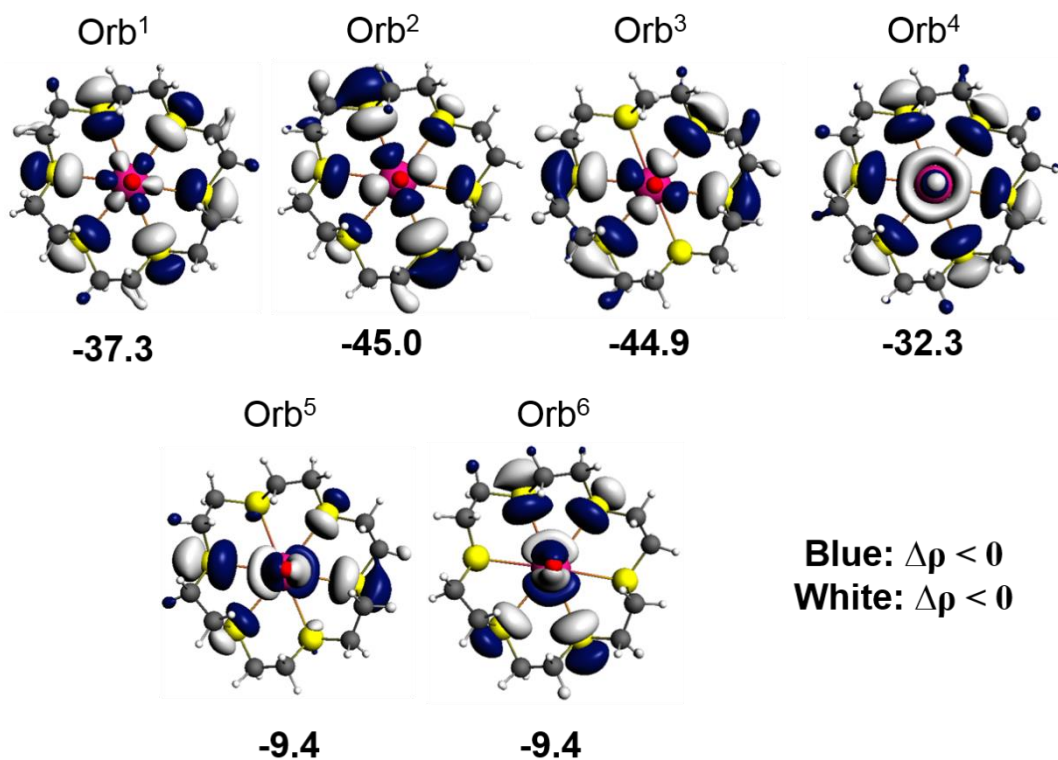


Figure 7. Plot of representative An-S_{L3} bonding interactions from ETS-NOCV method from an open-shell B3LYP calculation (energy unit: kcal/mol, isovalue=0.03).

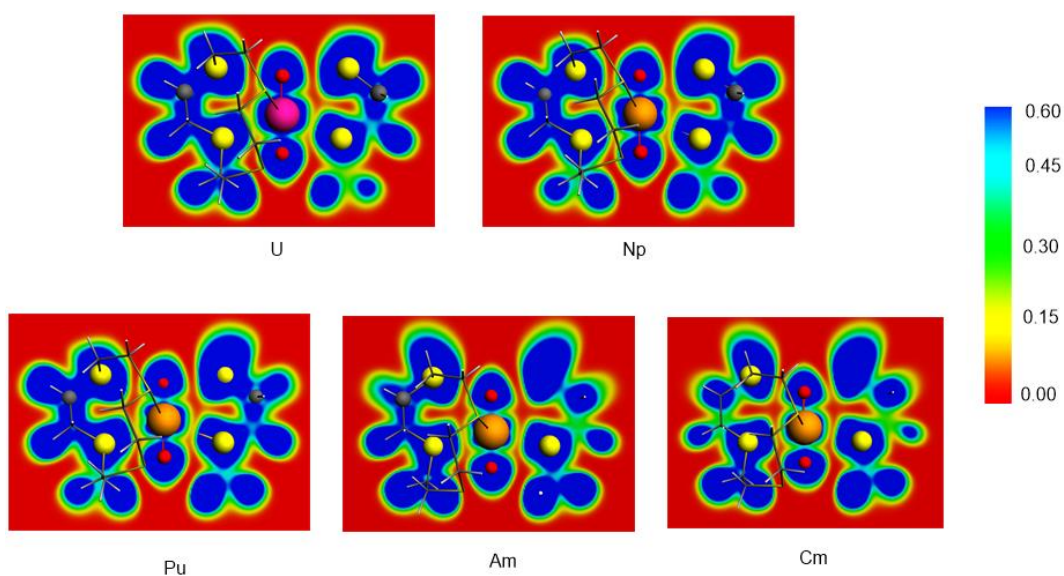


Figure 8. Two-dimensional ELF contours for the planes containing the four An-S_{L1} bonds in AnO₂²⁺(12TC4)₂. The results are based on the SR-ZORA PBE/T2ZP calculated densities.

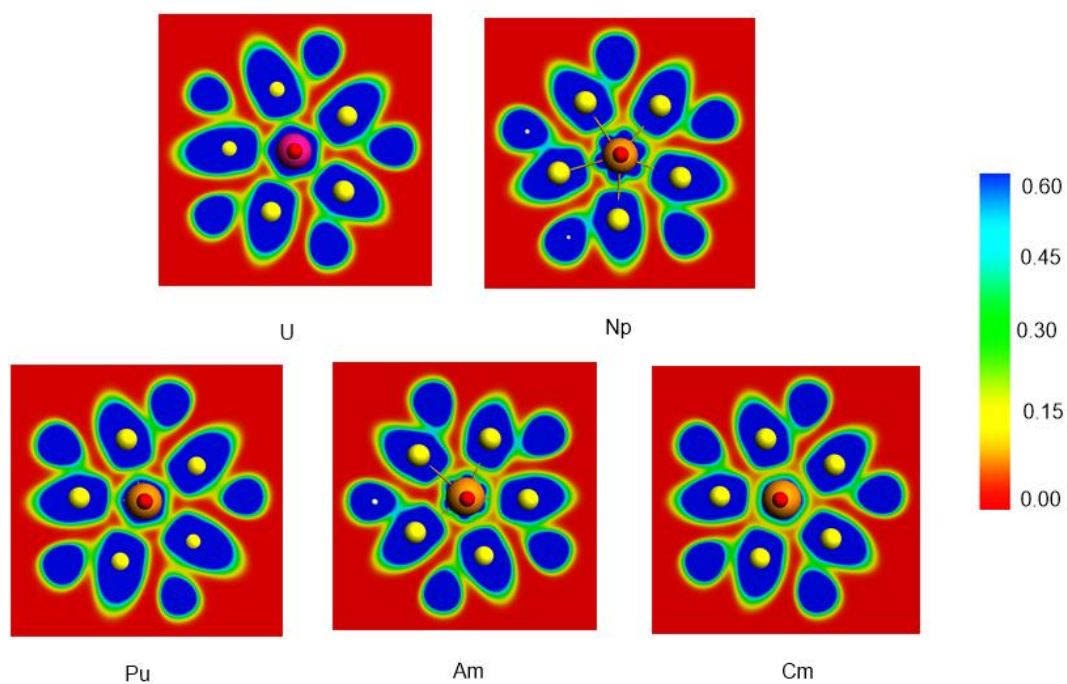


Figure 9. Two-dimensional ELF contours for the planes containing the five An-S L_2 bonds in AnO_2^{2+} (15TC5). The results are based on the SR-ZORA PBE/T2ZP calculated densities.

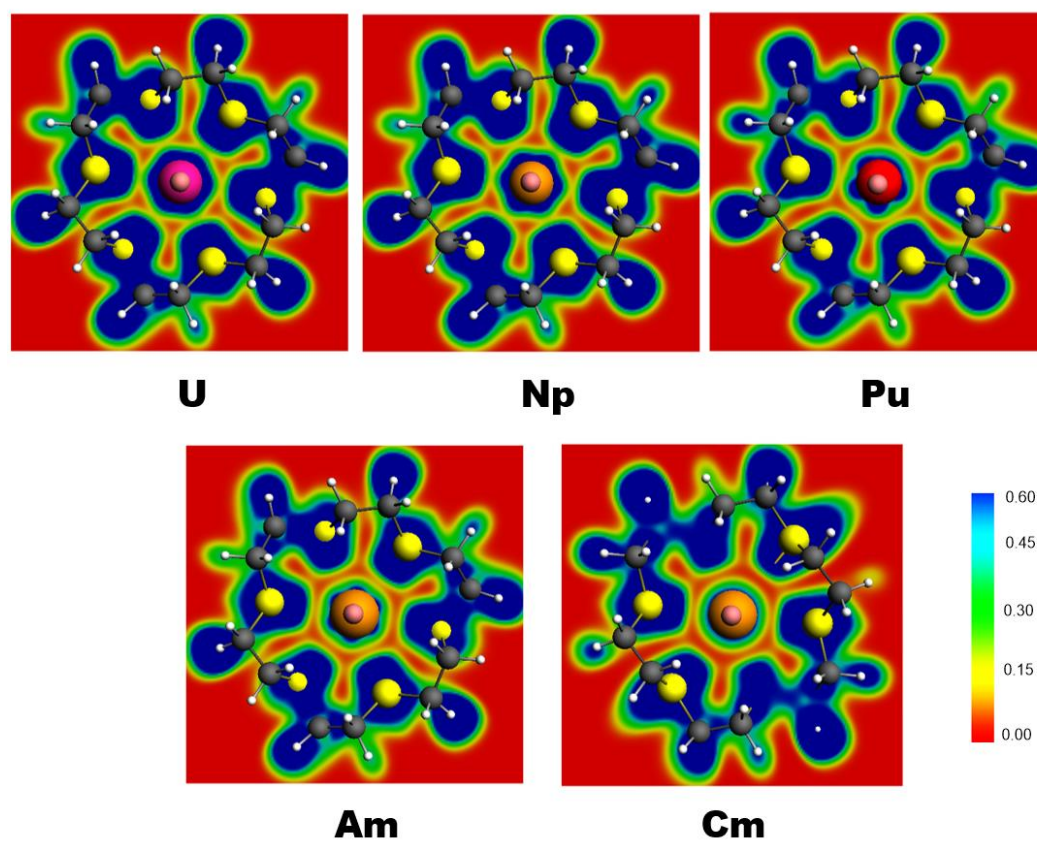


Figure 10. Two-dimensional ELF contours for the planes containing the six An-S L_3 bonds in AnO_2^{2+} (15TC5).

AnO_2^{2+} (18TC6). The results are based on the SR-ZORA PBE/TZ2P calculated densities.

A comprehensive assessment of the structure and bonding of these complexes was performed. Tables 7-9 list the bond distances, Mayer bond orders, and Mulliken charges of the $\text{AnO}_2(\text{L})^{2+}$ complexes calculated with PBE ZORA/TZ2P. The Mayer bond order shows An-O orders higher than 2, in good agreement with the generally accepted view that these bonds possess partial triple bond character. Although there is some triple bond character remains, reduction of the actinyl oxidation state from +VI to +V for An = U to Cm decreases the corresponding bond orders because the extra electron occupies a nonbonding f-orbital due to the energy level of 5f-orbital lying below that of the O-2p orbital. The Mayer bond orders for bonds between actinides and the equatorial sulfur ligands are substantially less than 1, with a decline trend of $\text{An-S}_{\text{L1}} > \text{An-S}_{\text{L2}} > \text{An-S}_{\text{L3}}$, attributed to the longer bond distances and the lesser actinide charge extension across the series. However, the complexes of actinyls with 15-thio-crown-5 and 18-thio-crown-6 have higher bond orders (U- S_{L2} bond orders of 0.44, U- S_{L3} bond orders of 0.38) than those complexes of actinyl with 15-crown-5 (U- O_{eq} bond orders of 0.36)[38] and 18-crown-6 (U- O_{eq} bond orders of 0.33)[71], due to the large extended radial distribution of the S-3p orbitals compared with the O-2p orbitals. Of particular importance is the trend that when upon proceeding across the actinide series, the An- S_{L} bond order and total binding energies generally decrease in parallel with a decrease in ionic bonding. This trend further confirmed that that reduced distance of the An- S_{L} bonds from An = U to Cm does not result in stronger bonding because the An- S_{L} bonds are dominated by ionic bonding that gradually decreases from An = U to Cm.

Table 7. Bond Length, Mayer Bond Orders, and Mulliken Charge and NPA charge of $\text{C}_2\text{AnO}_2(12\text{TC4})_2^{2+}$ (An = U, Np, Pu, Am and Cm) at the SR-PBE/TZ2P level.

Species	Bond Length		BondOrder		Mulliken		NPA	
	O-An	S-An	O-An	S-An	An	O	An	O
U	1.806	3.074	2.059	0.375	1.59	-0.52	1.16	-0.58
Np	1.799	3.085	2.007	0.348	1.59	-0.51	1.53	-0.31
Pu	1.777	3.055	1.931	0.309	1.79	-0.53	2.35	-0.39
Am	1.780	3.086	1.793	0.249	1.55	-0.43	3.08	-0.45
Cm	1.812	3.0222	1.671	0.236	1.78	-0.53	3.09	-0.45

Table 8. Average Bond Length, Mayer Bond Orders, and Mulliken Charges of $\text{AnO}_2(15\text{TC5})^{2+}$ (An = U, Np, Pu, Am and Cm) at the SR-PBE/TZ2P level.

	Bond Length, Å		Mayer Bond Order		Mulliken Charge		
	O-An	S-An	O-An	S-An	An	O	S
U	1.788	2.930	2.016	0.444	1.67	-0.55	0.23
Np	1.772	2.921	2.004	0.441	1.63	-0.53	0.23
Pu	1.767	2.915	1.985	0.439	1.62	-0.51	0.22
Am	1.765	2.906	1.979	0.417	1.56	-0.49	0.23
Cm	1.775	2.902	1.814	0.406	1.49	-0.47	0.23

Table 9. Average Bond Length, Mayer Bond Orders, and Mulliken Charges of $\text{AnO}_2(18\text{TC6})^{2+}$ (An = U, Np, Pu, Am and Cm) at the SR-PBE/TZ2P level.

	Bond Length, Å		Mayer Bond Order		Mulliken Charge		
	O-An	S-An	O-An	S-An	An	O	S
U	1.790	3.090	2.020	0.375	1.58	-0.55	0.20
Np	1.773	3.088	2.008	0.360	1.56	-0.53	0.20
Pu	1.768	3.080	1.992	0.348	1.58	-0.51	0.19
Am	1.768	3.098	1.958	0.313	1.52	-0.49	0.20
Cm	1.788	3.142	1.804	0.289	1.48	-0.50	0.20

Further insights into the electronic structure of the actinyl thio-crown ether complexes were obtained from natural localized bond orbital (NLMO) and natural population (NPA) analyses, the results of which are given in Table 10. The calculated NLMO results show that the thio-crown ether ligand has p-type lone pairs on the ether sulfur atoms, similar to the oxygen atoms of the 15-crown-5 ligand as shown in our previous work.[38] Upon coordination to AnO_2^{2+} , the An-S_L interactions are mainly ionic, with rather weak An-S_L covalent interactions which feature a decreasing trend of $\sigma_{\text{SL1-An}}$ bonding in the equatorial plane.

Table 10. The calculated natural localized molecular orbitals (NLMOs) of $\text{AnO}_2(12\text{TC4})_2^{2+}$, $\text{AnO}_2(15\text{TC5})_2^{2+}$ and $\text{AnO}_2(18\text{TC6})_2^{2+}$ (An = U, Np, Pu, Am and Cm) complexes.

Species	Type	Occ.	NLMO
$\text{AnO}_2(12\text{TC4})_2^{2+}$			
U	$\sigma_{\text{SL1-U}}$	4*1.91	89.1%S(sp ^{3.38}) + 10.9%U(s ^{0.4} d ^{0.8} f)
	$\pi_{\text{SL1-U}}$	4*1.92	96.1%S(sp ^{1.3}) + 2.4%U(d ^{1.1} f)
Np	$\sigma_{\text{SL1-Np}}$	4*1.93	88.4%S(sp ^{2.37}) + 10.2%Np(sd ^{2.5} f)
	$\pi_{\text{SL1-Np}}$	4*1.92	96.2%S(sp ^{1.9}) + 2.2%Np(d ² f)
Pu	$\sigma_{\text{SL1-Pu}}$	4*1.93	91.0%S(sp ^{2.2}) + 7.6%Pu(d ^{3.8} f)

	$\pi_{\text{SL1-Pu}}$	4*1.94	96.9% S(sp ^{2.0}) + 1.4% Pu(d ⁴ f)
Am	$\sigma_{\text{SL1-Am}}$	4*1.93	91.2% S(sp ^{2.4}) + 6.5% Am(d ^{4.8} f)
	$\pi_{\text{SL1-Am}}$	4*1.94	97.2% S(sp ^{1.8}) + 1.1% Am(d ^{6.8} f)
Cm	$\sigma_{\text{SL1-Cm}}$	4*1.94	90.6% O(sp ^{2.4}) + 8.0% Cm(sd ^{6.8} f)
	$\pi_{\text{SL1-Cm}}$	4*1.94	97.0% O(sp ^{1.8}) + 1.3% Cm(d ^{9.0} f)
AnO₂(15TC5)²⁺			
U	$\sigma_{\text{SL2-U}}$	5*1.87	81.3% S(sp ^{4.3}) + 16.6% U(s ^{0.6} d ^{2.1} f)
	$\pi_{\text{SL2-U}}$	5*1.92	97.8% S(sp) + 1.0% U(d ^{0.8} f)
Np	$\sigma_{\text{SL2-Np}}$	5*1.93	88.4% S(sp ^{2.37}) + 10.2% Np(sd ^{2.5} f)
	$\pi_{\text{SL2-Np}}$	5*1.92	96.2% S(sp ^{1.9}) + 2.2% Np(d ² f)
Pu	$\sigma_{\text{SL2-Pu}}$	5*1.93	91.0% S(sp ^{2.2}) + 7.6% Pu(d ^{3.8} f)
	$\pi_{\text{SL2-Pu}}$	5*1.94	96.9% S(sp ^{2.0}) + 1.4% Pu(d ⁴ f)
Am	$\sigma_{\text{SL2-Am}}$	5*1.90	85.1% S(sp ^{4.2}) + 13.1% Am(s ^{1.1} d ^{3.0} f)
	$\pi_{\text{SL2-Am}}$	5*1.94	98.0% S(sp) + 0.7% Am(d ^{2.2} f)
Cm	$\sigma_{\text{SL2-Cm}}$	5*1.90	86.7% S(sp ^{3.7}) + 11.7% Cm(s ^{1.2} d ^{3.7} f)
	$\pi_{\text{SL2-Cm}}$	5*1.96	98.0% S(sp ^{1.1}) + 0.7% Cm(d ^{2.6} f)
AnO₂(18TC6)²⁺			
U	$\sigma_{\text{SL3-U}}$	6*1.89	83.2% S(sp ^{4.8}) + 14.3% U(s ^{0.3} d ^{1.5} f)
	$\pi_{\text{SL3-U}}$	6*1.96	97.8% S(sp) + 0.7% U(df)
Np	$\sigma_{\text{SL3-Np}}$	6*1.89	84.6% S(sp ^{4.6}) + 13.0% Np(s ^{0.4} d ^{1.7} f)
	$\pi_{\text{SL3-Np}}$	6*1.96	97.9% S(sp) + 0.6% Np(d ^{1.5} f)
Pu	$\sigma_{\text{SL3-Pu}}$	6*1.93	91.0% S(sp ^{2.2}) + 7.6% Pu(d ^{3.8} f)
	$\pi_{\text{SL3-Pu}}$	6*1.94	96.9% S(sp ^{2.0}) + 1.4% Pu(d ⁴ f)
Am	$\sigma_{\text{SL3-Am}}$	6*1.98	84.0% S(p) + 15.8% Am(d ^{0.7} f)
	$\pi_{\text{SL3-Am}}$	6*1.96	98.1% S(sp) + 0.4% Am(d ^{4.6} f)
Cm	$\sigma_{\text{SL3-Cm}}$	6*1.92	89.8% S(sp ^{3.3}) + 8.6% Cm(s ^{1.7} d ^{5.3} f)
	$\pi_{\text{SL3-Cm}}$	6*1.82	98.6% S(sp ^{0.9}) + 0.2% Cm(d ^{7.1} f)

Conclusions

We have investigated the electronic and geometric structure of complexes formed between actinyls AnO₂²⁺, and thio-crown ether macrocyclic ligands using different quantum chemical methods. The agreement between the different approaches, as well as comparison to available experimental data (such as geometries, vibrational frequencies and reduction potentials) confirms the validity and accuracy of our methodology. Our evaluation of the coordination chemistry of actinyls with thio-crown ethers provides the following guidance: (1) The cavity of 12-thio-crown-4 ether is

too small to accommodate actinyl ions, while AnO_2^{2+} fit well into 5-thio-crown-5 ether and 18-thio-crown-6 ether to form a five-fold or six-fold coordinated An-S_L ionic bonds in the equatorial plane. (2) All those complexes formed by these ligands possess distorted geometries with a twist-like conformation of the ligand macrocycle. (3) An-S_L dative bonding is rather weak, and the change in the bond order is in the orderings of $L2 > L3$ and $U > \text{Np} > \text{Pu} > \text{Am} > \text{Cm}$. (4) The change-over of polarized An-O_{yl} bonding character from d transition element behavior to f inner-transition element behavior, here labeled as the americium turn, provides insights into the electronic structure of the actinides and provides elucidation of the effects of coordinating ligands on the An-O bonding relative to actinyl ions.

Acknowledgements

This work was supported by the National Natural Science Foundation of China (grant nos. 21433005, 91426302, and 21590792) [J.L.], by NASF (U1530401) [S.X.H.], and as part of the Center for Actinide Science and Technology (CAST) an Energy Frontier Research Center (EFRC) funded by the U.S. Department of Energy (DOE), Office of Science, Basic Energy Sciences (BES), under Award Number DE-SC0016568 [J.K.G.].

Notes and references

- [1] L.R. Morss, N.M. Edelstein, J. Fuger, in: Springer, Dordrecht, Springer: Dordrecht, The Netherlands, 2006.
- [2] J.D. Kubicki, G.P. Halada, P. Jha, B.L. Phillips, *Chem. Cent. J.*, 3 (2009) 1–29.
- [3] J. Li, B.E. Bursten, *J. Am. Chem. Soc.*, 119 (1997) 9021–9032.
- [4] N. Kaltsoyannis, *Inorg. Chem.*, 52 (2013) 3407–3413.
- [5] A.F. Lucena, S.O. Odoh, J. Zhao, J. Marcalo, G. Schreckenbach, J.K. Gibson, *Inorg. Chem.*, 53 (2014) 2163–2170.
- [6] S.X. Hu, J.K. Gibson, W.L. Li, M.J. Van Stipdonk, J. Martens, G. Berden, B. Redlich, J. Oomens, J. Li, *Chem. Comm.*, 52 (2016) 12761–12764.
- [7] J. Su, W.H.E. Schwarz, J. Li, *Inorg. Chem.*, 51 (2012) 3231–3238.
- [8] C. Vidaud, D. Bourgeois, D. Meyer, *Chem. Res. Toxicol.*, 25 (2012) 1161–1175.
- [9] X. Yang, Z.F. Chai, D.Q. Wang, *Phys. Chem. Chem. Phys.*, 17 (2015) 7537–7547.
- [10] J. Su, P.D. Dau, Y.H. Qiu, H.T. Liu, C.F. Xu, D.L. Huang, L.S. Wang, J. Li, *Inorg. Chem.*, 52 (2013) 6617–6626.
- [11] P. Pyykkö, L.L. Lohr, *Inorg. Chem.*, 20 (1981) 1950–1959.
- [12] W. Huang, W.H. Xu, W.H.E. Schwarz, J. Li, *Inorg. Chem.*, 55 (2016) 4616–4625.
- [13] Y. Kato, T. Kimura, Z. Yoshida, N. Nitani, *Radiochim. Acta*, 74 (1996) 21–25.
- [14] A.M. Fedosseev, A.V. Gogolev, I.A. Charushnikova, V.P. Shilov, *Radiochim. Acta*, 99 (2011) 679–686.
- [15] J.C. Eisenstein, M.H.L. Pryce, *Proceedings of the Royal Society of London A*, A238 (1956) 31.
- [16] J.C. Eisenstein, M.H.L. Pryce, *Journal of research of the National Institute of Standards*, 69A (1965) 217.

- [17] N. Jiang, W.H. Schwarz, J. Li, *Inorg. Chem.*, 54 (2015) 7171–7180.
- [18] A. Kovacs, R.J.M. Konings, J.K. Gibson, I. Infante, L. Gagliardi, *Chem. Rev.*, 115 (2015) 1725–1759.
- [19] J. Marcalo, J.K. Gibson, *J. Phys. Chem. A*, 113 (2009) 12599–12606.
- [20] P. Pyykkö, J. Li, N. Runeberg, *J. Phys. Chem.*, 98 (1994) 4809–4813.
- [21] A. Kovácsa, R.J.M. Konings, *J. Mol. Struct.: THEOCHEM*, 684 (2004) 35–42.
- [22] J.-B. Liu, G.P. Chen, W. Huang, D.L. Clark, W.H.E. Schwarz, J. Li, *Dalton Trans.*, 46 (2017) 2542–2550.
- [23] J. Su, P.D. Dau, H.T. Liu, D.L. Huang, F. Wei, W.H. Schwarz, J. Li, L.S. Wang, *J. Chem. Phys.*, 142 (2015) 134308.
- [24] T. Fujii, A. Uehara, Y. Kitatsuji, H. Yamana, *J. Radioanal. Nucl. Chem.*, 303 (2015) 1015–1020.
- [25] J.H. Lan, C.Z. Wang, Q.Y. Wu, S.A. Wang, Y.X. Feng, Y.L. Zhao, Z.F. Chai, W.Q. Shi, *J. Phys. Chem. A*, 119 (2015) 9178–9188.
- [26] G.A. Shamov, *J. Am. Chem. Soc.*, 133 (2011) 4316–4329.
- [27] Y.L. Wang, Z.Y. Liu, Y.X. Li, Z.L. Bai, W. Liu, Y.X. Wang, X.M. Xu, C.L. Xiao, D.P. Sheng, D.W. Juan, J. Su, Z.F. Chai, T.E. Albrecht-Schmitt, S. Wang, *J. Am. Chem. Soc.*, 137 (2015) 6144–6147.
- [28] B. Çiçek, A. Yıldız, *Molecules*, 16 (2011) 8670–8683.
- [29] G.R. Choppin, *J. Radioanal. Nucl. Chem.*, (2007) 695–703.
- [30] R.D. Rogers, C.B. Bauer, A.H. Bond, *J. Alloys. Compd.*, 213 (1994) 305-312.
- [31] R.D. Rogers, A.H. Bond, W.G. Hipple, A.N. Rollins, R.F. Henry, *Inorg. Chem.*, 30 (1991) 2671-2679.
- [32] G.W. Gokel, W.M. Leevy, M.E. Weber, *Chem. Rev.*, 104 (2004) 2723–2750.
- [33] Y. Gong, J.K. Gibson, *Inorg. Chem.*, 53 (2014) 5839–5844.
- [34] W. Zhou, X.L. Sun, L. Gu, F.F. Bao, X.X. Xu, C.Y. Pang, Z.G. Gu, Z.J. Li, *J. Radioanal. Nucl. Chem.*, 300 (2014) 843–852.
- [35] K.M. Doxsee, H.R. Wierman, T.J.R. Weakley, *J. Am. Chem. Soc.*, 114 (1992) 5165–5171.
- [36] P.G. Eller, R.A. Penneman, *Inorg. Chem.*, 15 (1976) 2439–2442.
- [37] V. Mougel, L. Chatelain, J. Pecaut, R. Caciuffo, E. Colineau, J.C. Griveau, M. Mazzanti, *Nature Chem.*, 4 (2012) 1011–1017.
- [38] S.-X. Hu, W.-L. Li, L. Dong, J.K. Gibson, J. Li, *Dalton Trans.*, 46 (2017) 12354–12363.
- [39] M.J. Frisch, G.W. Trucks, H.B. Schlegel, G.E. Scuseria, M.A. Robb, J.R. Cheeseman, G. Scalmani, V. Barone, B. Mennucci, G.A. Petersson, H. Nakatsuji, M. Caricato, X. Li, H.P. Hratchian, A.F. Izmaylov, J. Bloino, G. Zheng, J.L. Sonnenberg, M. Hada, M. Ehara, K. Toyota, R. Fukuda, J. Hasegawa, M. Ishida, T. Nakajima, Y. Honda, O. Kitao, H. Nakai, T. Vreven, J. Montgomery, J. A., J.E. Peralta, F. Ogliaro, M. Bearpark, J.J. Heyd, E. Brothers, K.N. Kudin, V.N. Staroverov, T. Keith, R. Kobayashi, J. Normand, K. Raghavachari, A. Rendell, J.C. Burant, S.S. Iyengar, J. Tomasi, M. Cossi, N. Rega, J.M. Millam, M. Klene, J.E. Knox, J.B. Cross, V. Bakken, C. Adamo, J. Jaramillo, R. Gomperts, R.E. Stratmann, O. Yazyev, A.J. Austin, R. Cammi, C. Pomelli, J.W. Ochterski, R.L. Martin, K. Morokuma, V.G. Zakrzewski, G.A. Voth, P. Salvador, J.J. Dannenberg, S. Dapprich, A.D. Daniels, Ö. Farkas, J.B. Foresman, J.V. Ortiz, J. Cioslowski, D.J. Fox, *Gaussian 09, Revision C.01*, (Wallingford CT: Gaussian, Inc. 2010).
- [40] E.J. Baerends, D.E. Ellis, P. Ros, *Chem. Phys.*, 2 (1973) 41–51.
- [41] E.J. Baerends, (et al., *ADF2013, SCM*, Theoretical Chemistry, Vrije Universiteit, Amsterdam, The Netherlands, <http://www.scm.com>).
- [42] R.S. Mulliken, *J. Chem. Phys.*, 23 (1955) 1833–1840.
- [43] E.J. Baerends, V. Branchadell, M. Sodupe, *Chem. Phys. Lett.*, 265 (1997) 481–489.
- [44] J.P. Perdew, M. Emzerhof, K. Burke, *J. Chem. Phys.*, 105 (1996) 9982–9985.
- [45] E. Vanlenthe, E.J. Baerends, J.G. Snijders, *J. Chem. Phys.*, 99 (1993) 4597–4610.
- [46] E. van Lenthe, E.J. Baerends, J.G. Snijders, *J. Chem. Phys.*, 101 (1994) 9783–9792.
- [47] E. van Lenthe, E.J. Baerends, *J. Comput. Chem.*, 24 (2003) 1142–1156.
- [48] A. Klamt, G. Schüürmann, *J. Chem. Soc.-Perkin Trans. 2*, 0 (1993) 799–805.

- [49] N.L. Allinger, X.F. Zhou, J. Bergsma, *J. Mol. Struct.: THEOCHEM*, 312 (1994) 69–83.
- [50] A. Michalak, M. Mitoraj, T. Ziegler, *J. Phys. Chem. A*, 112 (2008) 1933–1939.
- [51] L. Versluis, T. Ziegler, *J. Chem. Phys.*, 88 (1988) 322–328.
- [52] M. Mitoraj, A. Michalak, T. Ziegler, *Organometallics*, 28 (2009) 3727–2733.
- [53] R.F. Nalewajski, J. Mrozek, *Int. J. Quantum Chem.*, 51 (1994) 187–200.
- [54] R.F. Nalewajski, J. Mrozek, A. Michalak, *Int. J. Quantum Chem.*, 61 (1997) 589–601.
- [55] I. Mayer, *Chem. Phys. Lett.*, 97 (1983) 270–274.
- [56] A. Michalak, R.L. De Kock, T. Ziegler, *J. Phys. Chem. A*, 112 (2008) 7256–7263.
- [57] M. Mitoraj, A. Michalak, *J. Mol. Model.*, 13 (2007) 347–355.
- [58] P. de Silva, J. Korchowiec, T.A. Wesolowski, *ChemPhysChem*, 13 (2012) 3462–3465.
- [59] M. Dolg, U. Wedig, H. Stoll, H. Preuss, *J. Chem. Phys.*, 86 (1987) 866–872.
- [60] X. Cao, M. Dolg, H. Stoll, *J. Chem. Phys.*, 118 (2003) 487–496.
- [61] X. Cao, M. Dolg, *J. Mol. Struct.*, 673 (2004) 203–209.
- [62] R.A. Kendall, T.H. Dunning Jr., R.J. Harrison, *J. Chem. Phys.*, 96 (1992) 6796–6806.
- [63] A.D. Becke, *J. Chem. Phys.*, 98 (1993) 5648–5652.
- [64] C.T. Lee, W.T. Yang, R.G. Parr, *Phys. Rev. B*, 37 (1988) 785–789.
- [65] A.E. Reed, L.A. Curtiss, F. Weinhold, *Chem. Rev.*, 88 (1988) 899–926.
- [66] A.E. Reed, R.B. Weinstock, F. Weinhold, *J. Chem. Phys.*, 83 (1985) 735–746.
- [67] R. Krishnan, J.S. Binkley, R. Seeger, J.A. Pople, *J. Chem. Phys.*, 72 (1980) 650–654.
- [68] E.D. Glendening, J.K. Badenhoop, A.E. Reed, J.E. Carpenter, J.A. Bohmann, C.M. Morales, F. Weinhold, NBO 5.0, (Theoretical Chemistry Institute, University of Wisconsin, Madison, 2001).
- [69] P. Pyykkö, *The Journal of Physical Chemistry A*, 119 (2015) 2326–2337.
- [70] M. Straka, K.G. Dyall, P. Pyykkö, *Theor. Chem. Acc.*, 106 (2001) 393–403.
- [71] G.A. Shamov, G. Schreckenbach, *J. Phys. Chem. A*, 110 (2006) 9486–9499.